Adv. Manuf. (2019) 7:30–41
https://doi.org/10.1007/s40436-018-0243-8

Physical-based constitutive model considering the microstructure evolution during hot working of AZ80 magnesium alloy

Ze-Xing Su[1,2] · Chao-Yang Sun[1,2] · Ming-Wang Fu[3] · Ling-Yun Qian[1,2]

Received: 23 May 2018 / Accepted: 7 December 2018 / Published online: 2 January 2019
© The Author(s) 2018

Abstract A physical-based constitutive model was developed to model the viscoplastic flow behavior and microstructure evolution of AZ80 magnesium alloy during the hot working process. The competing deformation mechanisms, including work hardening, dynamic recovery, and dynamic recrystallization, in an isothermal compression environment were considered in the model. The internal state variables, including the normalized dislocation density and recrystallized volume fraction, were incorporated into the model to articulate the microstructure evolution during hot deformation. The kinetic condition critical for dynamic recrystallization, considering the effects of the deformation temperature and strain rate, was obtained by employing both the Poliak-Jonas criterion and Zener-Hollomon parameter. Microstructure observations indicate that the recrystallized volume fraction increases with decreasing Z parameter at constant strain, which is consistent with the predicted kinetics model. Based on the developed model, a good correlation was also obtained between the predicted and experimental flow stress. The results indicate a good predictability of the model in describing the hot deformation behavior and microstructure evolution of AZ80 magnesium alloy.

✉ Chao-Yang Sun
suncy@ustb.edu.cn

[1] School of Mechanical Engineering, University of Science and Technology Beijing, Beijing 100083, People's Republic of China

[2] Beijing Key Laboratory of Lightweight Metal Forming, Beijing 100083, People's Republic of China

[3] Department of Mechanical Engineering, The Hong Kong Polytechnic University, Hung Hom, Hong Kong, People's Republic of China

Keywords AZ80 magnesium alloy · Hot deformation · Constitutive model · Microstructure evolution · Dynamic recrystallization (DRX)

1 Introduction

Magnesium alloy is one of the most promising lightweight metallic materials for structural applications in the automotive and aerospace industries owing to its low density, high specific strength, and good recyclability [1, 2]. However, the slip systems of the alloy are poor at room temperature due to its hexagonal close-packed (HCP) structure, which limits its deformation and manufacturability and thus its application in the industry [3, 4]. To improve the workability of the alloy, plastic deformation, such as extrusion and forging, is usually conducted at elevated temperatures, which increases the number of slip planes and decreases the critical shear stress of non-basal plane slip [5]. During the hot deformation of magnesium alloy, dynamic recrystallization (DRX) predominates because of its low stacking fault energy (60–78 mJ/m^2), which is an effective way to obtain a refined microstructure and improve the mechanics performance [6]. The understanding of the flow behavior and metallurgical phenomena during hot deformation is of scientific significance for the optimization of the hot workability and guiding forming process of magnesium alloy.

A constitutive model is essential for the description of the flow characteristics of materials, which could be combined with a finite element method to provide an efficient computational platform for the prediction of the mechanical response. Over the past decades, numerous constitutive models have been established such as phenomenological models, e.g., Arrhenius-type model and

Johnson-Cook model [7, 8], advanced statistical models, e.g., artificial neural network model [9, 10], and physical-based internal state variable (ISV) models, e.g., Zerilli-Armstrong model and Kocks-Mecking model [11, 12]. By modeling of the deformation process, Liu and Ding [13] established an Arrhenius-type constitutive model for AZ91 magnesium alloy to describe the hot deformation behavior for a wide range of temperatures and strain rates. Sabokpa et al. [14] developed an artificial neural network (ANN) model for the representation of the hot compression behavior of AZ81 magnesium alloy and compared it with the Arrhenius-type model. The results indicated that the trained ANN model was more accurate in predicting the flow stress. Furthermore, Li et al. [15] conducted a comparative study on Arrhenius-type, ANN, and modified Zerilli-Armstrong models to predict the hot deformation behavior of T24 steel. The ANN model showed the most excellent predictability. However, it was pointed out that the ANN model strongly depended on extensive high-quality data and characteristic variables did not provide physical insights.

Among the different models, the phenomenological model is currently the most widely used one due to the few parameters and simplicity in determining the parameters by regression analysis. However, the model presents a poor predictability in determining deformation parameters that are not in the experimental range. The advanced statistical model is the most accurate in predicting the flow behavior of a wide range of deformation conditions. However, the model does not have an intrinsic physics meaning and cannot reflect the microstructure evolution during the deformation. Compared with the above-mentioned models, the physical-based ISV approach has become more important in modeling various flow behaviors and microstructure evolution over the past decades.

The constitutive ISV model is capable of capturing inherent microstructural complexity during the working process and achieving a reasonable accuracy, which can be used in computational simulation for process optimization [16]. Vilamosa et al. [17] established a physical-based constitutive model for AA6082 aluminum alloy using the dislocation density as an internal variable without relating it to microstructure evolution. Austin and Mcdowell [18] proposed a dislocation-based constitutive model for the viscoplastic deformation of fcc metals at high strain rates by introducing path-dependent differential equations for mobile and immobile dislocation densities. Lin et al. [19] developed a dislocation-based unified viscoplastic constitutive model for C–Mn steel to predict the dislocation density, recrystallization, and grain size evolution during multi-pass hot rolling processing. The aforementioned study is a good reference and basis for establishing the physical-based constitutive model for AZ80 magnesium alloy to describe the flow behavior and microstructure evolution during the hot working process.

At present, many constitutive models, which are available for magnesium alloys, are generally phenomenologically constructed by introducing a few macroscopic variables to the model and formulated as functions of the temperature, strain rate and strain. They are basically experimental and based on classical viscoplastic theory to describe work hardening and thermal softening phenomena during the hot working process. However, the models lack an in-depth understanding of the underlying physics. In view of the important role of DRX in the grain refinement and improvement of mechanical properties during the hot working of magnesium alloy, the establishment of a constitutive model that can reflect the evolution of the recrystallized microstructure is urgently needed. In this study, a physical-based constitutive model was established by introducing ISVs including the normalized dislocation density and recrystallized volume fraction. To provide an adequate description of the recrystallization kinetics, the Poliak-Jonas criterion and the Zener-Hollomon parameter were employed because they represented the microstructure evolution, which was simultaneously affected by the deformation temperature and strain rate. The model was verified using the experimental flow stress and recrystallized volume fraction and a good agreement was observed. The proposed constitutive model can be used to analyze the hot deformation behavior and microstructure evolution of AZ80 magnesium alloy.

2 Experimental procedures

The as-received AZ80 magnesium alloy is an extruded billet with a diameter of 200 mm and a height of 150 mm. The chemical composition (mass fraction) of the alloy is: 8.16% Al, 0.42% Zn, 0.03% Mn, 0.01% Si, 0.005% Fe, 0.001% Cu, 0.001% Ni, and balance Mg. According to the standard of ASTM E209 [20] for compression tests of metallic materials at elevated temperatures with conventional or rapid heating rates and strain rates, cylindrical specimens with a diameter of 8 mm and height of 12 mm were machined from the extruded bar along the extrusion direction. Two end surfaces of the specimens were ground to reduce the effect of friction on the hot deformation behavior. A uniaxial hot compression test was conducted with a Gleeble-1500D thermomechanical simulator; the schematic is illustrated in Fig.1. Five deformation temperatures (300, 325, 350, 375 and 400 °C) and three strain rates (0.001, 0.01 and 0.1 s^{-1}) were used and the height reduction was 60%, corresponding to a true strain of 0.916. Before the compression, the top and bottom surfaces of the specimens were coated with graphite lubricant and

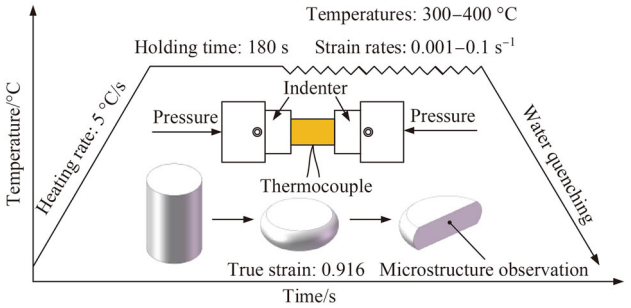

Fig. 1 Schematic illustration of isothermal compression tests for AZ80 magnesium alloy

tantalum foil was placed between the specimen and anvil to reduce the friction and avoid adhesion. For the measurement and feedback control of the real-time temperature, K-type thermocouples were welded in the center of specimens. The specimens were heated to the test deformation temperature with a heating rate of 5 °C/s and then held isothermally for 180 s to eliminate the thermal gradient prior to the deformation. Stress-strain data were automatically recorded by the testing system during the hot deformation process. After the compression, the specimens were immediately water-quenched to retain the deformation microstructure.

The deformed specimens were sectioned along the compression axis for microstructural analysis using a wire-electric discharge machine (EDM). The sectioned specimens were mechanically ground, polished, and then etched for 5–12 s using a solution consisting of 5 mL picric acid, 5 mL acetic acid, 100 mL ethyl alcohol, and 10 mL distilled water. Microstructure observations were made with a DM4000M optical microscope. The average grain size and recrystallized volume fraction were examined by quantitative metallography.

3 Experimental results and analysis

The true compressive stress-strain response of AZ80 magnesium alloy is shown in Fig. 2. Despite the difference in the specific flow stress, the flow response presents a peak stress with subsequent flow softening, which is a typical DRX characteristic. In general, the variation in the flow stress reflects the competition between work hardening (WH) and dynamic softening during hot deformation. The flow stress firstly rapidly increases due to dislocation tangling and pileups and dynamic recovery (DRV) simultaneously arises through dislocation climbing and gliding, which results in the formation of mobile subgrain boundaries and the annihilation of dislocations. As the dislocation density exceeds a threshold, DRX nucleates at low-angle grain boundaries. Therefore, the flow stress decreases dramatically by further dislocation annihilation. When the dislocation proliferation and annihilation achieve a dynamic equilibrium, the flow characteristics affected by strain hardening and dynamic softening maintain a steady state.

Note that the flow stress has a negative sensitivity to the temperature and a positive sensitivity to the strain rate. High temperature leads to a much higher driving energy for dislocation movement, while a low strain rate provides sufficient time for DRV and DRX, which both contribute to the decrease in the flow stress. It can be concluded that the dynamic softening stage starts at a lower strain and flow softening more likely occurs at an increased deformation temperature and decreased strain rate because both the abundant energy and sufficient time affect the thermal activation process including DRV and DRX.

4 Constitutive ISV model

4.1 Flow stress decomposition

According to Hooke's law, the stress-strain relationship of materials can be expressed as [21]

$$\sigma = E\left(\varepsilon_{\mathrm{T}} - \varepsilon_{\mathrm{p}}\right), \tag{1}$$

where σ is the overall flow stress; E is the Young' modulus, which is a temperature-dependent parameter; and ε_{T} and ε_{p} represent the total strain and plastic strain, respectively.

Because the material exhibits viscoplastic flow during the hot working process, the overall flow stress can be decomposed into three parts: initial yield stress, viscoplastic stress, and hardening stress [22]

$$\sigma = k + \sigma_{\mathrm{v}} + H, \tag{2}$$

where k is the initial yield stress, σ_{v} the viscoplastic stress, and H the isotropic hardening stress. A hyperbolic sine law is introduced to describe the viscoplastic flow, which is suitable for a wide range of temperatures and strain rates [23, 24]

$$\dot{\varepsilon}_{\mathrm{p}} = A_1 \sinh^{n_{\mathrm{c}}}\left(A_2(\sigma - H - k)\right), \tag{3}$$

where $\dot{\varepsilon}_{\mathrm{p}}$ is the plastic strain rate; n_{c} is the viscoplastic exponent, which is temperature-dependent; and A_1 and A_2 are material constants.

The hardening stress H in Eq.(3) has a close relationship with the reciprocal of the average slip length over which a dislocation can run and the mean slip length is determined by the inverse square of the dislocation density [25]. The isotropic hardening rate can thus be defined as [26, 27]

$$\dot{H} = 0.5B\bar{\rho}^{-0.5}\dot{\bar{\rho}}, \tag{4}$$

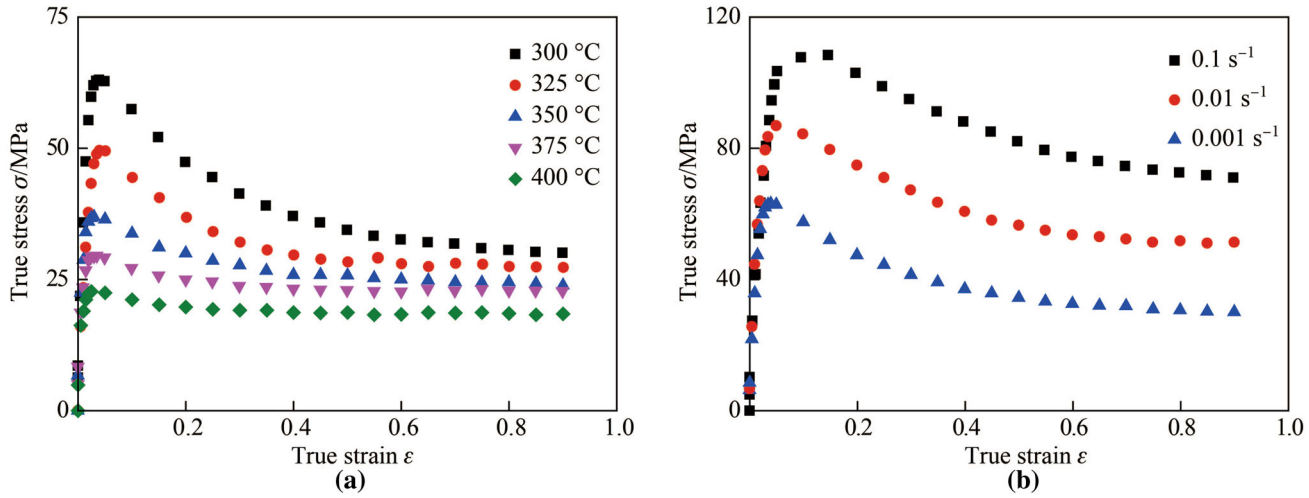

Fig. 2 True stress-strain response obtained from hot compression of AZ80 magnesium alloy under **a** different temperatures at 0.001 s^{-1}, and **b** different strain rates at 300 °C

where B is a temperature-dependent parameter; $\bar{\rho}$ is the normalized dislocation density formulated as $\bar{\rho} = 1 - \rho_0/\rho$ [28]; ρ_0 is the initial dislocation density, and ρ is the dislocation density during the deformation process. The $\bar{\rho}$ value varying from 0 to 1 represents the dislocation that evolves from the initial state to the saturated state.

The initial yield stress k in Eq.(3) is temperature-dependent and decreases with increasing temperature. It can be expressed by an Arrhenius-type equation: $k = k_0 \exp(Q_k/RT)$. The parameters k_0 and Q_k are the material constant and activation energy of k, respectively.

4.2 Dislocation density evolution

During high temperature deformation, dislocation multiplication and trapping by existing obstacles provide a driving force for DRV and DRX. Considering the hot deformation mechanisms, the evolution of the dislocation density can be described as [19]

$$\dot{\bar{\rho}} = A_4(1-\bar{\rho})|\dot{\varepsilon}_P|^{\delta_2} - C_r\bar{\rho}^{\delta_3} - \left((A_3\bar{\rho})\Big/(1-S)^{\delta_4}\right)\dot{S}, \quad (5)$$

where A_3, A_4, δ_2, δ_3, and δ_4 are material constants and C_r is a temperature-dependent parameter. The first term represents the accumulation and DRV of the dislocation density. The DRV part limits the normalized dislocation density to the saturated state of a dislocation network when $\bar{\rho} = 1$. The second term models the static recovery during the heating process. The third term expresses the effect of DRX on the evolution of the dislocation density and S is the recrystallized volume fraction.

4.3 Dynamic recrystallization kinetics

The DRX plays an extremely important role in thermo-mechanical processing, affecting the final microstructure and mechanical properties of the deformed magnesium alloys. The critical condition for the initiation of DRX usually depends on the Zener-Hollomon parameter (Z parameter) based on empirical equations [29]. The Z parameter represents the effects of the temperature and strain rate on the deformation behavior and can be expressed as $Z = \dot{\varepsilon}\exp(Q/RT)$. The deformation activation energy Q can be estimated by fitting the peak stress with a hyperbolic sine function [30]

$$A(\sinh(\alpha\sigma))^n = \dot{\varepsilon}\exp(Q/RT), \quad (6)$$

where $\dot{\varepsilon}$ is the true strain rate (s^{-1}), and A, n, and α are material constants obtained from linear regression based on the Arrhenius-type equation [31]. Based on the regression analysis of the $\ln(\sinh(\alpha\sigma))$ versus $1/T$ diagram under different strain rates and Eq. (7), the value of Q is 142.054 kJ/mol

$$Q = nR\frac{\partial(\ln(\sinh(\alpha\sigma)))}{\partial(1/T)}. \quad (7)$$

At a constant initial grain size, the peak strain ε_h and critical strain ε_c can usually be described with a power-law function of Z ($\varepsilon = KZ^m$) [32], where K and m are material constants. The peak strain can be obtained from the flow stress curve. To determine the critical strain for DRX, the irreversible thermodynamic principle proposed by Poliak and Jonas [33] was employed

$$\frac{\partial}{\partial\sigma}\left(-\frac{\partial\theta}{\partial\sigma}\right) = 0, \quad (8)$$

where θ is the strain hardening rate and is determined by $\theta = \frac{\partial \sigma}{\partial \varepsilon}$.

Based on the Poliak-Jonas criterion, the onset of DRX can be identified from an inflection point of the strain hardening rate θ as a function of the flow stress σ. Because of the following equation,

$$\left(\frac{\partial \theta}{\partial \sigma}\right)_{\dot{\varepsilon}} = \left(\frac{\partial \ln \theta}{\partial \varepsilon}\right)_{\dot{\varepsilon}}. \tag{9}$$

The $\ln\theta$ versus ε curve should also exhibit an inflection when DRX takes place. The critical strain of DRX is then mathematically obtained by combining the inflection point criterion of $\ln\theta$ versus ε curve with the minimum value criterion of $-\frac{\partial(\ln\theta)}{\partial\varepsilon}$ versus ε curve. This provides an intuitionistic description for the analysis of the effect of the deformation conditions on the recrystallized critical strain, as shown in Fig. 3. Figure 3 shows that the critical strain decreases with increasing deformation temperature and decreasing strain rate, which illustrates that a higher temperature and lower strain rate are more conducive to the occurrence of DRX.

Accordingly, the critical and peak strains as functions of the Z parameter can be expressed by a linear regression in logarithmic form (see Fig. 4a)

$$\begin{cases} \varepsilon_c = 2.81 \times 10^{-3} Z^{0.113}, \\ \varepsilon_h = 3.27 \times 10^{-3} Z^{0.114}. \end{cases} \tag{10}$$

The critical strain was confirmed to be a function of the peak strain ($\varepsilon_c \cong 0.79\varepsilon_h$), as shown in Fig. 4b, which is consistent with the results for a wide range of materials [34–36].

When the dislocation density increases to a critical value, nucleation and growth of the DRX nucleus will preferentially occur at high dislocation density zones such as deformation bands and grain boundaries [37]. To describe the evolution of DRX and predict the recrystallized volume fraction, a rate equation is proposed [25]

$$\dot{S} = Q_0 \bar{\rho}(x\varepsilon - \varepsilon_c(1-S))(1-S)^{\delta_1}, \tag{11}$$

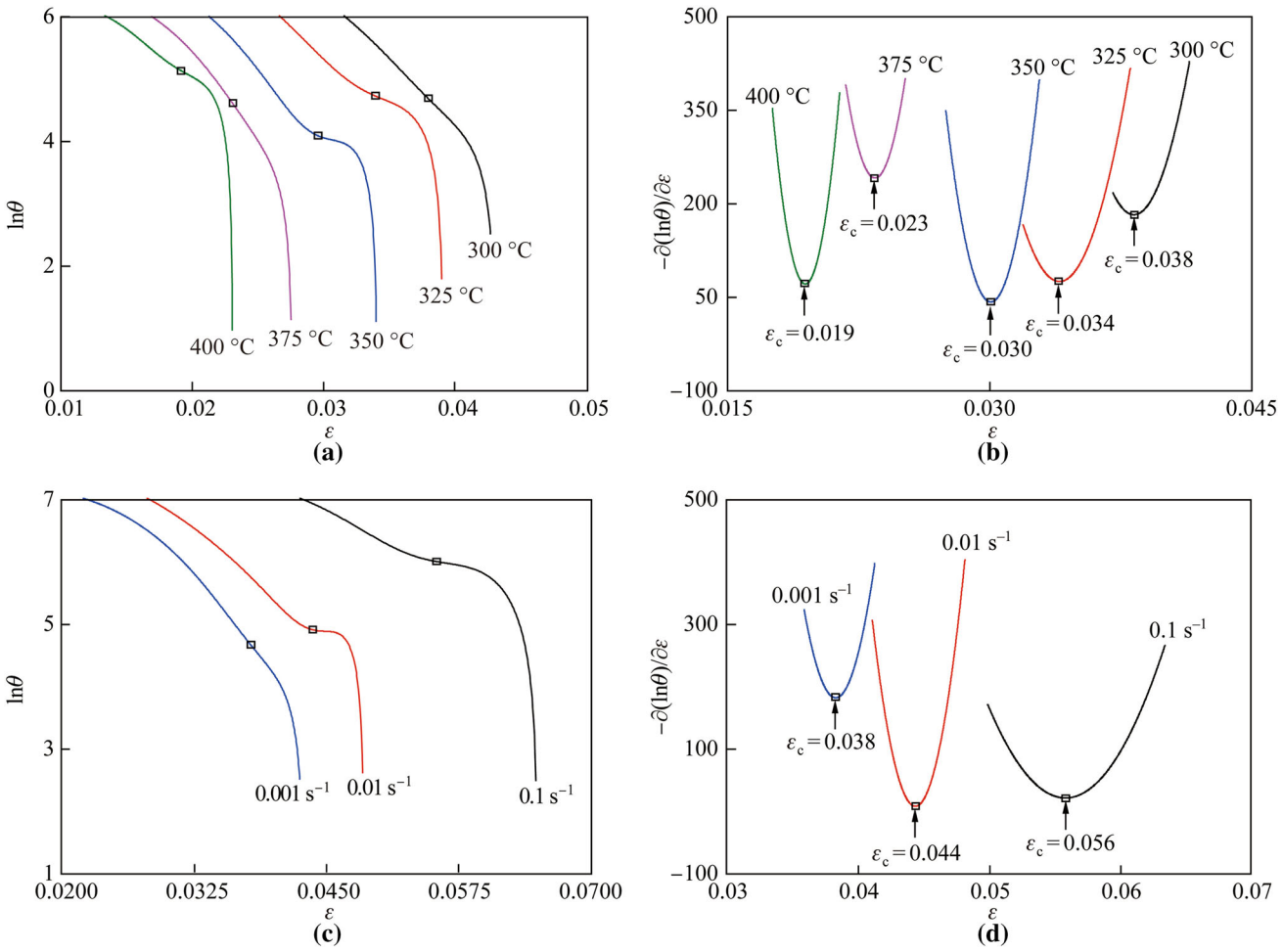

Fig. 3 Plots of $\ln\theta$ versus ε and $-\frac{\partial(\ln\theta)}{\partial\varepsilon}$ versus ε to determine the critical strain of DRX under **a**, **b** different temperatures at 0.001 s^{-1}; **c**, **d** different strain rates at 300 °C

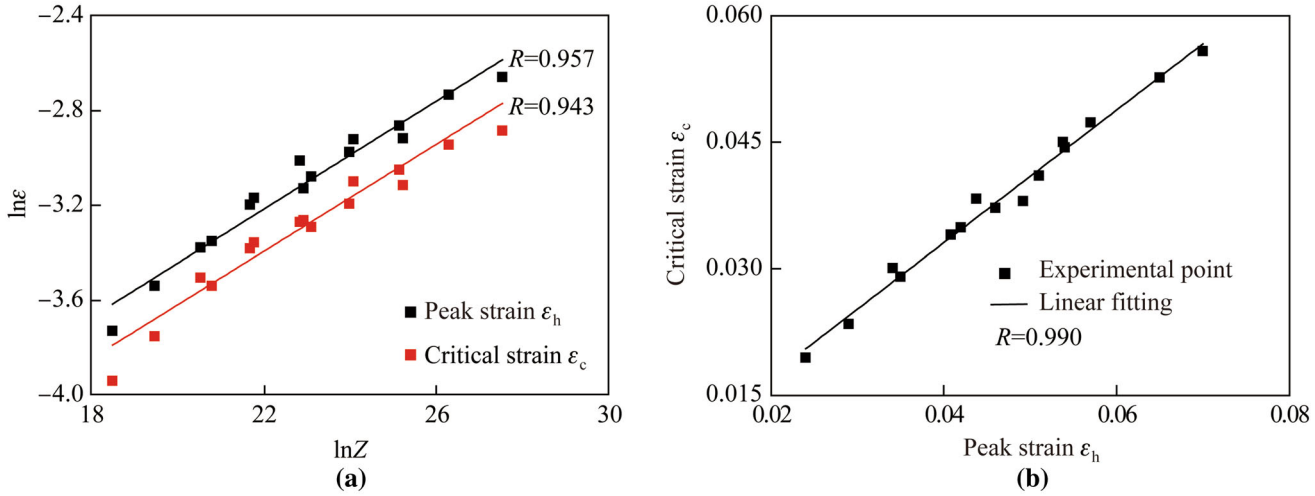

Fig. 4 Critical and peak strains **a** as functions of Z parameter and **b** the linear fitting relationship between the critical and peak strains

where δ_1 is a material constant and Q_0 is a temperature-dependent parameter. The recrystallized volume fraction S varies from 0 to 1 and its variation is cyclic, depending on the evolution of the dislocation density.

It has been proven experimentally that an incubation time is needed for the onset of recrystallization, which can be expressed as [38]

$$\dot{x} = A_0(1-x)\bar{\rho}, \tag{12}$$

where $\dot{x}$ is the incubation fraction and A_0 is a temperature-dependent parameter.

4.4 Constitutive model development

Because the microstructure evolution including hardening, recovery, and recrystallization mechanisms is considered, a set of physical-based viscoplastic constitutive ISV equations can be formulated for AZ80 magnesium alloy

$$\begin{cases} \dot{\varepsilon}_{\mathrm{p}} = A_1 \sinh^{n_{\mathrm{c}}}(A_2(\sigma - H - k)), \\ \dot{S} = Q_0\bar{\rho}(x\varepsilon - \varepsilon_{\mathrm{c}}(1-S))(1-S)^{\delta_1}, \\ \dot{x} = A_0(1-x)\bar{\rho}, \\ \dot{H} = 0.5B\bar{\rho}^{-0.5}\dot{\bar{\rho}}, \\ \dot{\bar{\rho}} = A_4(1-\bar{\rho})|\dot{\varepsilon}_{\mathrm{P}}|^{\delta_2} - C_{\mathrm{r}}\bar{\rho}^{\delta_3} - \left((A_3\bar{\rho})\Big/(1-S)^{\delta_4}\right)\dot{S}, \\ \sigma = E\left(\varepsilon_{\mathrm{T}} - \varepsilon_{\mathrm{p}}\right). \end{cases} \tag{13}$$

Under high-temperature conditions, the deformation is temperature-dependent due to atom diffusion and dislocation motion. The material parameters in the constitutive model are treated as temperature-dependent parameters, which can be expressed as Arrhenius-type equations

$$\begin{cases} E = E_0 \exp(Q_{\mathrm{E}}/RT), \\ n_{\mathrm{c}} = n_0 \exp(Q_{\mathrm{n}}/RT), \\ B = B_0 \exp(Q_{\mathrm{b}}/RT), \\ k = k_0 \exp(Q_{\mathrm{k}}/RT), \\ C_{\mathrm{r}} = C_{\mathrm{r}_0} \exp(-Q_{\mathrm{c}}/RT), \\ Q_0 = Q_{10} \exp(-Q_{\mathrm{Q}}/RT), \\ A_0 = A_{00} \exp(-Q_{A00}/RT), \end{cases} \tag{14}$$

where R is the universal gas constant (8.314 (J·K)/mol) and T is the absolute temperature (K). The Q in the exponential function denotes the activation energy for the corresponding material constants. To determine the material constants within the equations, a genetic algorithm (GA)-based optimization method was developed and programmed by minimizing the residuals of the experimental and calculated stress-strain data. A GA toolbox in Matlab software was used to optimize the objective function and determine the material constants. The details of the optimization process are reported in Refs. [39, 40]. The values determined for the material constants are listed in Table 1.

4.5 Constitutive model validation

The experimental and predicted stress-strain data for different deformation conditions are compared in this section. The results for the strain rates of 0.1 and 0.01 s^{-1} are shown in Fig. 5. Most of the experimental points are close to the predicted results, indicating a preferable prediction performance of the constitutive model. However, with increasing strain rate (see Fig.5a), the deviation increases at deformation temperatures of 300, 325 and 350 °C, especially in the work hardening-dynamic recovery stage. The predicted flow stresses agree well with the measured ones at higher deformation temperatures. The main reason for this phenomenon is that the predicted dynamic recovery

Table 1 Determined constants of the ISV viscoplastic constitutive model

E_0/MPa	n_0(–)	B_0/MPa	k_0/MPa	C_{r0}(–)	Q_{10}/(J·mol^{-1})
440	0.003	2.3	2.4	3.2	30 787.08
Q_E/(J·mol^{-1})	Q_n/(J·mol^{-1})	Q_b/(J·mol^{-1})	Q_k/(J·mol^{-1})	Q_C/(J·mol^{-1})	Q_Q/(J·mol^{-1})
25 000	37 000	17 800	1000	15 000	56 622.4
Q_{A00}/(J·mol^{-1})	δ_1(–)	δ_2(–)	δ_3(–)	δ_4(–)	A_{00}(–)
384.56	0.99	0.85	0.8	0.99	10
A_1(–)	A_2(–)	A_3(–)	A_4(–)		
7×10^{-5}	0.32	18	14.77		

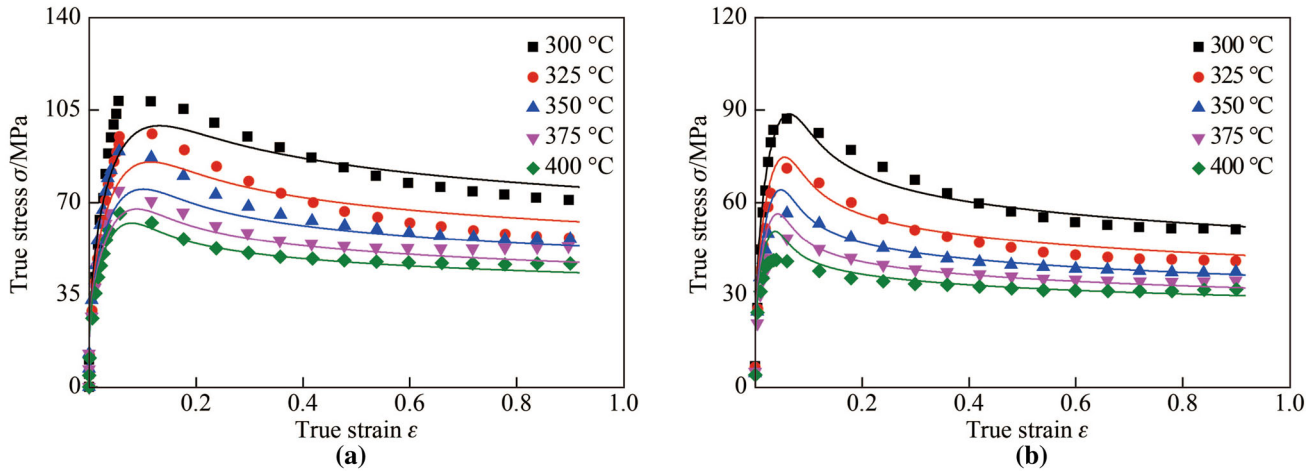

Fig. 5 Comparison of the experimental (symbols) and the predicted (solid curves) stress-strain data at the strain rate of **a** 0.1 s^{-1} and **b** 0.01 s^{-1}

rate is higher than the measured one. It is well known that magnesium alloy is a type of low stacking fault energy alloy; the dynamic recovery rate is low in the alloy because of the reduced mobility of the dislocations. A large grain boundary migration rate is induced by high local gradients of the dislocation density. Therefore, there is not enough time for the transformation of subgrains to grains, especially at higher strain rates, e.g., 0.1 s^{-1} [41]. On the other hand, the precipitate phase could also play an important role in the hot deformation behavior of AZ80 magnesium alloy. At low deformation temperatures (300, 325 and 350 °C), which are below the temperature of complete dissolution of the precipitate phase, the phase can strengthen the alloy due to the pinning effect of the grain boundaries and dislocations [42]. An excessive deformation resistance is therefore induced and the experimental flow stress shows a notable work hardening effect. With increasing temperature, the flow stress becomes insensitive to the deformation temperature due to the dissolution of the precipitate phase [2]. Thus, the actual dynamic recovery rate is low, resulting in the deviation between the measured and predicted flow stresses.

To evaluate the predictability of the proposed model, the correlation coefficient (R) and average absolute relative error (e_{AARE}) are specified

$$R = \frac{\sum_{i=1}^{n}(E_i - \bar{E})(P_i - \bar{P})}{\sqrt{\sum_{i=1}^{n}(E_i - \bar{E})^2 (E_i - \bar{E})}}, \tag{15}$$

$$e_{\mathrm{AARE}} = \frac{1}{n}\sum_{i=1}^{n}\left|\frac{E_i - P_i}{E_i}\right|, \tag{16}$$

where E_i and P_i are the experimental and predicted flow stress, respectively; $\bar{E}$ and $\bar{P}$ are the average values of E_i and P_i; and n is the number of sampling data. The values of R and e_{AARE} were calculated to be 96.0% and 5.9%, respectively, which indicated a good prediction accuracy of the model.

5 Results and discussion

The curves predicted for the dislocation density evolution exhibit rapid hardening to a single peak at relatively low strain and then flow softening followed by a steady state at high strain, as shown in Fig. 6. These characteristics are consistent with the variation in the flow stress in Fig. 2. It can be concluded that the low strain rate and high deformation temperature benefit dislocation annihilation and lead to a decreasing dislocation density and increasing mobile dislocations. During the hot deformation, many of the dislocations are concentrated on the grain boundaries in the slip process. With increasing dislocation density near the grain boundaries, DRX takes place in the local area and then evolves into the interior of the grains. Consequently, both the dislocation density and flow stress are reduced by dislocation rearrangement and annihilation.

The curves predicted for the recrystallized volume fraction increase with the strain in a sigmoidal manner, as shown in Figs. 7a–c. The points marked as (1)–(5) represent the experimental data obtained from microstructure observations in Fig. 8 and are in good agreement with the predicted results. It is notable that the recrystallized volume fraction increases with increasing temperature at a given strain rate, while it decreases with increasing strain rate at a constant temperature. This is attributed to the higher mobility at grain boundaries at higher temperature and lower strain rate, which benefits the activation of DRX [43]. After the deformation reaches a critical strain, DRX occurs and the recrystallized volume fraction increases quickly with increasing strain until a considerable fraction of the microstructure is recrystallized.

As stated in our previous research [44], there is a close relationship between the recrystallized microstructure evolution and Z parameter. To explain the DRX kinetics in detail, microstructure observations were conducted under various Z values (corresponding to five specific deformation conditions), as shown in Fig. 8. Based on the following equation, $Z = \dot{\varepsilon}\exp(Q/RT)$, a low Z value corresponds to a high temperature and low strain rate, while a high Z value reflects a low temperature and high strain rate. An inhomogeneous microstructure with an average grain size of 35 μm is characteristic for the pre-extruded alloy, as shown in Fig. 8a. Figure 8b shows that new grains nucleate at the original grain boundaries. Subsequently, nucleation occurs at the growing grains, forming a necklace-type structure of grains. In this case, which corresponds to high Z conditions and low recrystallization kinetics, the nucleation of the recrystallized grains starts at a very high strain, leading to a notably incomplete recrystallized microstructure. At a low Z value with high recrystallization kinetics and mobility of grain boundaries, new grains bulge from the preexisting grain boundaries and grow quickly and adequately, forming a completely recrystallized microstructure (see Fig. 8f).

The statistical data of the recrystallized volume fraction under different Z values are presented in Fig. 7d. For a given strain of 0.916, the recrystallized volume fraction is less than 90% at high Z values, corresponding to an incomplete recrystallized microstructure (see Figs. 8b and c). On the other hand, full evolution of the recrystallized microstructure occurs at low Z values (see Figs. 8d–f); an almost 100% recrystallized volume fraction is shown in Fig. 7d. Based on the statistical analysis, it can be concluded that the recrystallized volume fraction increases with decreasing Z value for a given true strain, which can be confirmed by the predicted recrystallized kinetics shown in Figs. 7a–c. Similar features of the DRX microstructure during hot deformation were observed for other magnesium alloys [45, 46].

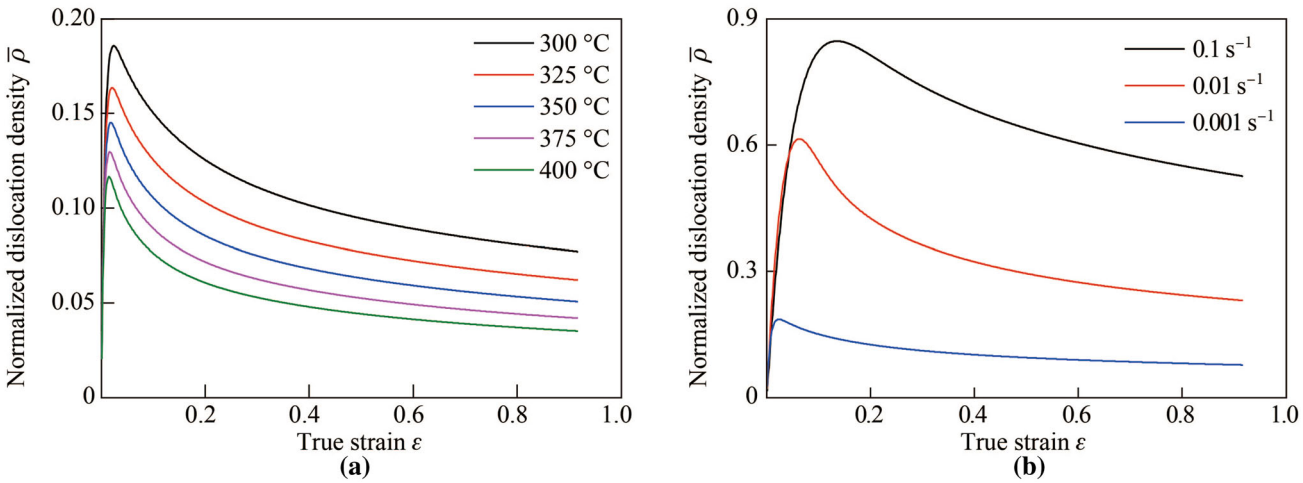

Fig. 6 Evolution of the normalized dislocation density under **a** different temperatures at 0.001 s^{-1}, and **b** different strain rates at 300 °C

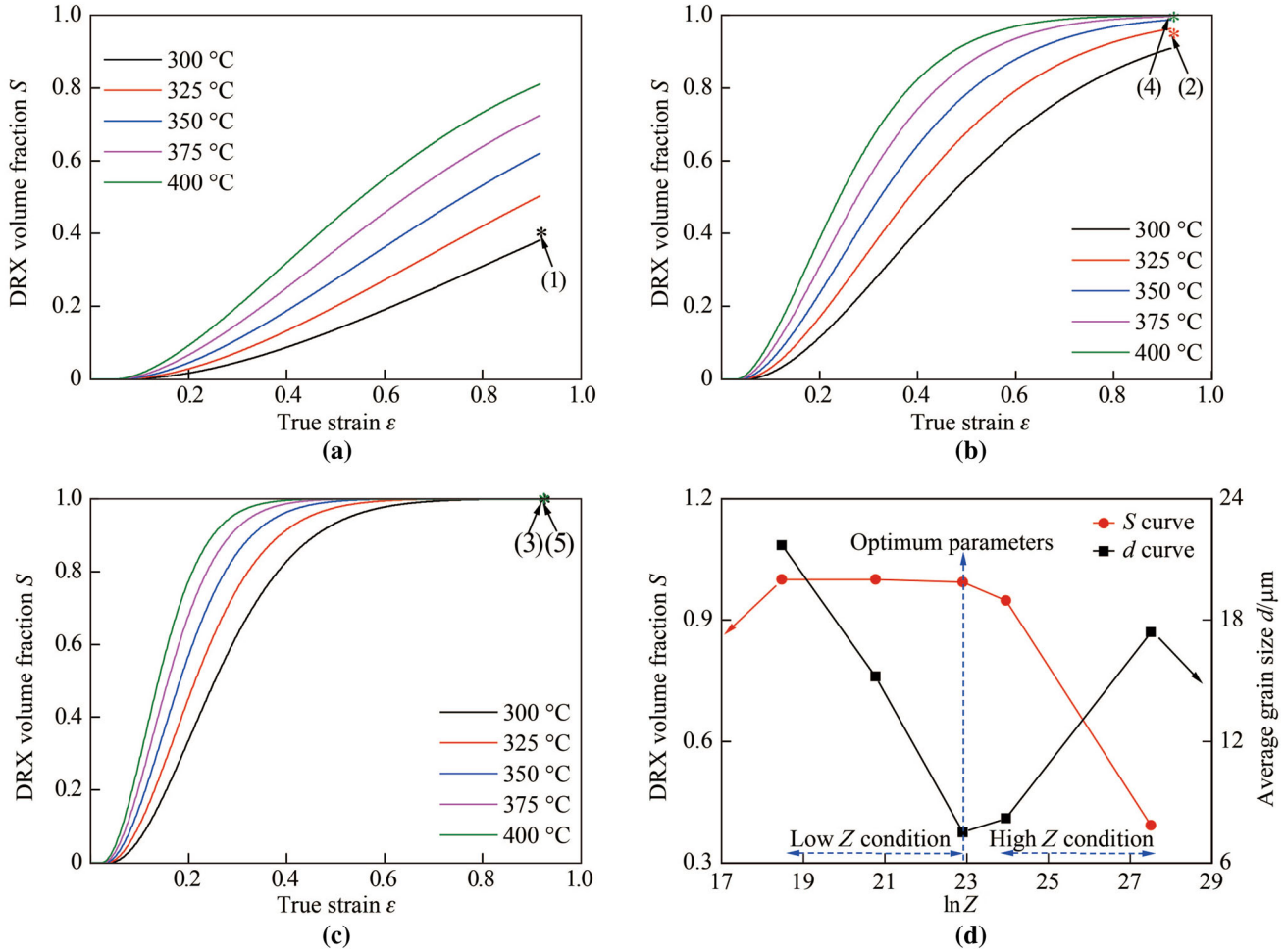

Fig. 7 Recrystallized volume fraction at the strain rate of **a** 0.1 s^{-1}, **b** 0.01 s^{-1} and **c** 0.001 s^{-1} (the curves represent the predicted values of the model, and the points marked with (1)–(5) represent the experimental values corresponding to the microstructures in Figs. 8b–f, respectively) **d** the statistical recrystallized volume fraction and the average grain size as a function of the logarithm of Z parameter

Another notable phenomenon under different Z conditions is the statistical result for the grain size distribution in the final microstructure (see Fig. 7d). Under high Z conditions with a high strain rate effect, work hardening is significant and the initiation of the recrystallization process is delayed. Consequently, the stored deformation energy is mostly used for the formation of new recrystallized grains and the average grain size becomes small and limited because there is no sufficient time for grain growth, which results in an inhomogeneous microstructure with an average grain size of 8.2 μm (see Fig. 8c). Under low Z conditions with a high temperature effect, some grains evolve quickly due to grain growth and grain impingement, which is consistent with an inhomogeneous microstructure with an average grain size of 15.2 μm (see Fig. 8e). Figure 8d shows a homogeneous and refined microstructure with an average grain size of 7.5 μm. Deformation conditions of 300 °C/0.001 s^{-1} correspond to a low ln$Z$ value of 22.9, which is plotted as vertical blue dashed line in Fig. 7d. It can thus be concluded that the low strain rate contributes to high recrystallization kinetics of 99.4%. The grains can maintain a small size under the low temperature, which is an optimum state for the hot working process. To achieve the desired final properties with an optimum microstructure (higher volume fraction of DRX grains and lower average grain size), a predetermined deformation temperature and strain rate should be considered.

6 Conclusions

(i) The DRX is the dominant softening mechanism in AZ80 magnesium alloy during the hot deformation process and its flow response exhibits a single peak followed by steady-state flow. The critical DRX strain was determined as a function of the peak strain

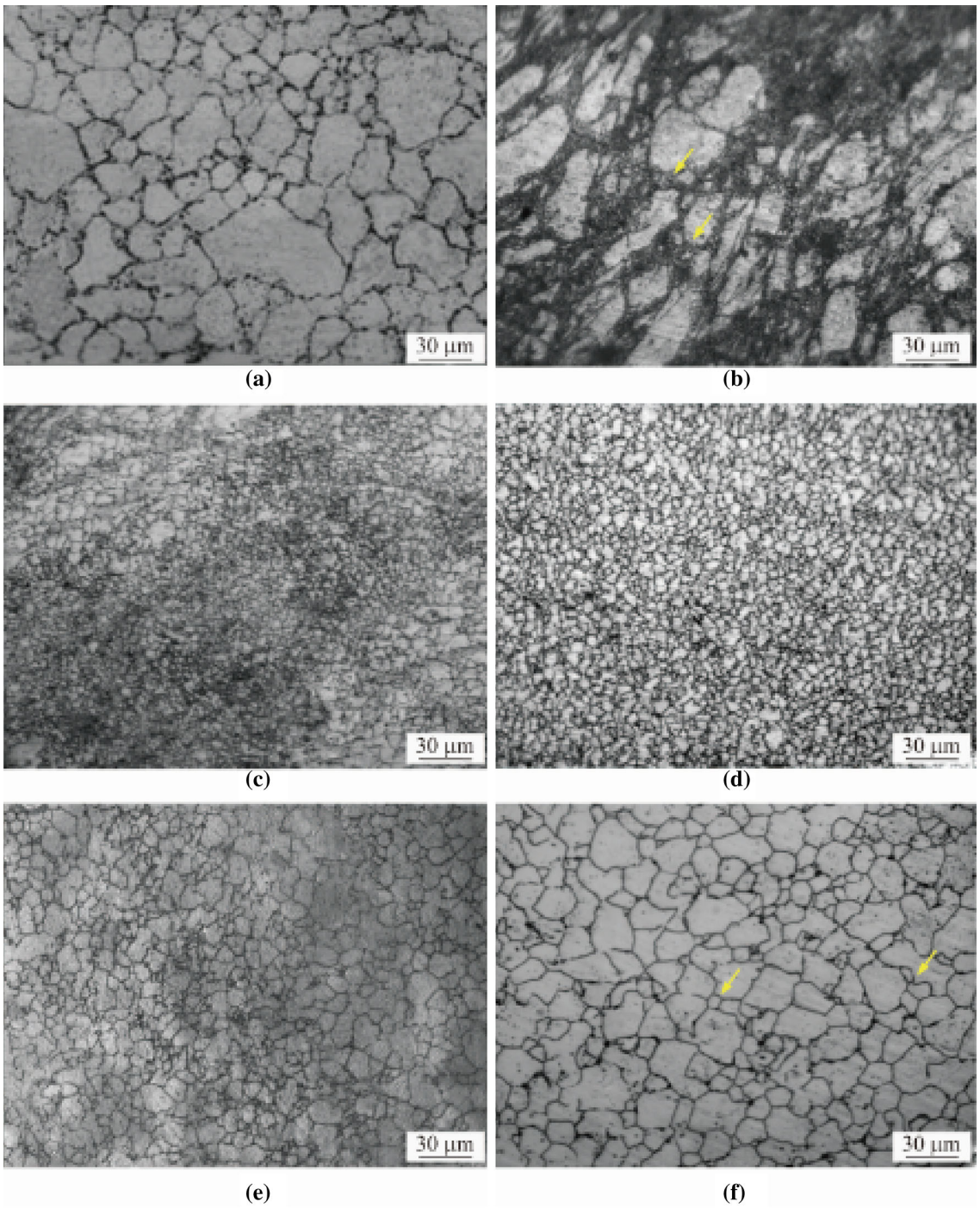

Fig. 8 Microstructures of **a** the pre-extruded state and the hot deformed state with a strain of 0.916 corresponding to the high Z value of **b** 300 °C/0.1 s^{-1} and **c** 325 °C/0.01 s^{-1}, the low Z value of **d** 300 °C/0.001 s^{-1}, **e** 400 °C/0.01 s^{-1} and **f** 400 °C/0.001 s^{-1}

based on the Poliak-Jonas criterion, which shows a power-law function of the Z parameter. A low Z value with high temperature and low strain rate is favorable for the occurrence of DRX.

(ii) A physical-based constitutive model was developed in consideration of work hardening, recovery, and DRX. The proposed model was built with ISVs including the normalized dislocation density, recrystallized volume fraction, and macroscopic variable Z parameter. Consequently, the viscoplastic flow behavior and microstructure evolution during the hot working process can be characterized.

(iii) The stress-strain data predicted by the constitutive model show a good correlation with the

experimental results. Statistical microstructure observations indicate an increase in the recrystallized volume fraction with decreasing Z parameter, which is consistent with the predicted recrystallized kinetics data. The model shows a good predictability in describing the hot deformation behavior and microstructure evolution of AZ80 magnesium alloy.

Acknowledgements The work is financially supported by the Natural Science Foundation of Beijing Municipality (Grant No. 3182025), the National Natural Science Foundation of China (Grant No. U1730121), the Joint Foundation (general) Project of the Equipment Pre-research of the Ministry of Education (Grant No. 6141A020221) and the Postdoctoral Science Foundation of China (Grant No. 2017M620609).

Open Access This article is distributed under the terms of the Creative Commons Attribution 4.0 International License (http://creativecommons.org/licenses/by/4.0/), which permits unrestricted use, distribution, and reproduction in any medium, provided you give appropriate credit to the original author(s) and the source, provide a link to the Creative Commons license, and indicate if changes were made.

References

1. Yu ZW, Tang AT, He JJ et al (2018) Effect of high content of manganese on microstructure, texture and mechanical properties of magnesium alloy. Mater Charact 136:310–317
2. Cai Y, Wan L, Guo ZH et al (2017) Hot deformation characteristics of AZ80 magnesium alloy: Work hardening effect and processing parameter sensitivities. Mater Sci Eng A 687:113–122
3. Roostaei M, Shirdel M, Parsa MH et al (2016) Microstructural evolution and grain growth kinetics of GZ31 magnesium alloy. Mater Charact 118:584–592
4. Tsao LC, Huang YT, Fan KH (2014) Flow stress behavior of AZ61 magnesium alloy during hot compression deformation. Mater Des 53(1):865–869
5. Das S, Barekar NS, Fakir OE et al (2015) Effect of melt conditioning on heat treatment and mechanical properties of AZ31 alloy strips produced by twin roll casting. Mater Sci Eng A 620:223–232
6. Jiang JJ, Song M, Yan HG et al (2016) Deformation induced dynamic recrystallization and precipitation strengthening in an Mg-Zn-Mn alloy processed by high strain rate rolling. Mater Charact 121:135–138
7. Zhou X, Wang M, Fu Y et al (2017) Effect of borides on hot deformation behavior and microstructure evolution of powder metallurgy high borated stainless steel. Mater Charact 124:182–191
8. Li HY, Li YH, Wang XF et al (2013) A comparative study on modified Johnson Cook, modified Zerilli-Armstrong and Arrhenius-type constitutive models to predict the hot deformation behavior in 28CrMnMoV steel. Mater Des 49:493–501
9. Li MQ, Xiong A, Li X (2006) An adaptive constitutive model of the Ti-6.29Al-2.71Mo-1.42Cr alloy in high-temperature deformation. J Mater Eng Perform 15(1):9–12
10. Duan YH, Ma LS, Qi HR et al (2017) Developed constitutive models, processing maps and microstructural evolution of Pb-Mg-10Al-0.5B alloy. Mater Charact 129:353–366
11. He A, Xie GL, Zhang HL et al (2014) A modified Zerilli-Armstrong constitutive model to predict hot deformation behavior of 20CrMo alloy steel. Mater Des 56:122–127
12. Momeni A, Ebrahimi GR, Jahazi M et al (2014) Microstructure evolution at the onset of discontinuous dynamic recrystallization: a physics-based model of subgrain critical size. J Alloy Compd 587:199–210
13. Liu LF, Ding HL (2009) Study of the plastic flow behaviors of AZ91 magnesium alloy during thermomechanical processes. J Alloy Compd 484(1–2):949–956
14. Sabokpa O, Zarei-Hanzaki A, Abedi HR et al (2012) Artificial neural network modeling to predict the high temperature flow behavior of an AZ81 magnesium alloy. Mater Des 39:390–396
15. Li HY, Wang XF, Wei DD et al (2012) A comparative study on modified Zerilli-Armstrong, Arrhenius-type and artificial neural network models to predict high-temperature deformation behavior in T24 steel. Mater Sci Eng A 536:216–222
16. Grong Ø, Shercliff HR (2002) Microstructural modelling in metals processing. Prog Mater Sci 47(2):163–282
17. Vilamosa V, Clausen AH, Børvik T et al (2016) A physically-based constitutive model applied to AA6082 aluminium alloy at large strains, high strain rates and elevated temperatures. Mater Des 103:391–405
18. Austin RA, Mcdowell DL (2011) A dislocation-based constitutive model for viscoplastic deformation of fcc metals at very high strain rates. Int J Plast 27(1):1–24
19. Lin J, Liu Y, Farrugia DCJ et al (2005) Development of dislocation-based unified material model for simulating microstructure evolution in multipass hot rolling. Philos Mag 85(18):1967–1987
20. Standard practice for compression tests of metallic materials at elevated temperatures with conventional or rapid heating rates and strain rates, astm. https://www.astm.org/DATABASE.CART/STD_REFERENCE/E9.htm. Accessed 23 May 2018
21. Lin J, Dean TA (2005) Modelling of microstructure evolution in hot forming using unified constitutive equations. J Mater Process Technol 167(2):354–362
22. Xiao WC, Wang BY, Wu Y et al (2017) Constitutive modeling of flow behavior and microstructure evolution of AA7075 in hot tensile deformation. Mater Sci Eng A 712:704–713
23. Huo YM, Bai Q, Wang BY et al (2015) A new application of unified constitutive equations for cross wedge rolling of a high-speed railway axle steel. J Mater Process Technol 223(223):274–283
24. Zhou J, Wang BY, Huang MD (2014) Two constitutive descriptions of boron steel 22MnB5 at high temperature. Mater Des 63(2):738–748
25. Ji HC, Liu JP, Wang BY et al (2017) Microstructure evolution and constitutive equations for the high-temperature deformation of 5Cr21Mn9Ni4N heat-resistant steel. J Alloy Compd 693:674–687
26. Mohamed MS, Foster AD, Lin J et al (2012) Investigation of deformation and failure features in hot stamping of AA6082: experimentation and modelling. Int J Mach Tools Manuf 53(1):27–38
27. Garrett RP, Lin J, Dean TA (2005) An investigation of the effects of solution heat treatment on mechanical properties for AA 6xxx alloys: experimentation and modelling. Int J Plast 21(8):1640–1657
28. Lin J, Liu Y (2003) A set of unified constitutive equations for modelling microstructure evolution in hot deformation. J Mater Process Technol 143(1):281–285
29. Huang K, Logé RE (2016) A review of dynamic recrystallization phenomena in metallic materials. Mater Des 111:548–574
30. Zhang J, Di H, Wang X et al (2013) Constitutive analysis of the hot deformation behavior of Fe-23Mn-2Al-0.2C twinning

induced plasticity steel in consideration of strain. Mater Des 44:354–364
31. Li MG, Xiao SL, Xu LJ et al (2018) Mechanical properties, deformation behavior and microstructure evolution of Ti-43Al-6Nb-1Mo-1Cr alloys. Mater Charact 136:69–83
32. Dehghan-Manshadi A, Barnett MR, Hodgson PD (2008) Hot deformation and recrystallization of austenitic stainless steel: Part II post-deformation recrystallization. Metall Mater Trans A 39(6):1371–1381
33. Poliak EI, Jonas JJ (2003) Initiation of dynamic recrystallization in constant strain rate hot deformation. Isij Int 43(5):684–691
34. Liu J, Cui Z, Ruan L (2011) A new kinetics model of dynamic recrystallization for magnesium alloy AZ31B. Mater Sci Eng A 529(1):300–310
35. Wan ZP, Sun Y, Hu LX et al (2017) Experimental study and numerical simulation of dynamic recrystallization behavior of TiAl-based alloy. Mater Des 122:11–20
36. Han Y, Wu H, Zhang W et al (2015) Constitutive equation and dynamic recrystallization behavior of as-cast 254SMO super-austenitic stainless steel. Mater Des 69:230–240
37. Lin YC, Chen XM, Wen DX et al (2014) A physically-based constitutive model for a typical nickel-based superalloy. Comput Mater Sci 83(2):282–289
38. Tang XF, Wang BY, Zhang N et al (2015) Modeling of microstructural evolution and flow behavior of superalloy IN718 using physically based internal state variables. Rare Met. https://doi.org/10.1007/s12598-015-0602-6
39. Cao J, Lin J (2008) A study on formulation of objective functions for determining material models. Int J Mech Sci 50(2):193–204
40. Sun CY, Guo N, Fu MW et al (2016) Experimental investigation and modeling of ductile fracture behavior of TRIP780 steel in hot working conditions. Int J Mech Sci 110:108–115
41. Montheillet F, Thomas JP (2004) Dynamic recrystallization of low stacking fault energy metals. Metall Mater High Struct Effic 146:357–368
42. Jiang LY, Huang WJ, Zhang DF et al (2017) Effect of Sn on the microstructure evolution of AZ80 magnesium alloy during hot compression. J Alloy Compd 727:205–214
43. Raghunath BK, Raghukandan K, Karthikeyan R et al (2011) Flow stress modeling of AZ91 magnesium alloys at elevated temperature. J Alloy Compd 509(15):4992–4998
44. Su ZX, Wan L, Sun CY et al (2016) Hot deformation behavior of AZ80 magnesium alloy towards optimization of its hot workability. Mater Charact 122:90–97
45. Fatemi-Varzaneh SM, Zarei-Hanzaki A, Beladi H (2007) Dynamic recrystallization in AZ31 magnesium alloy. Mater Sci Eng A 456(1):52–57
46. Xu Y, Hu LX, Sun Y (2013) Deformation behaviour and dynamic recrystallization of AZ61 magnesium alloy. J Alloy Compd 580(8):262–269